Young stars raining through the galactic halo: the nature and orbit of price-whelan 1

Michele Bellazzini, Rodrigo Ibata, Nicolas F. Martin, Khyati Malhan, Antonino Marasco, Benoit Famaey

Monthly Notices
of the
ROYAL ASTRONOMICAL SOCIETY

MNRAS **490,** 2588–2598 (2019)
Advance Access publication 2019 October 04

doi:10.1093/mnras/stz2788

Young stars raining through the galactic halo: the nature and orbit of price-whelan 1

Michele Bellazzini [1]★ Rodrigo A. Ibata,[2] Nicolas Martin,[2,3] Khyati Malhan,[4] Antonino Marasco [5,6] and Benoit Famaey [2]

[1]*INAF - Osservatorio di Astrofisica e Scienza dello Spazio, via Gobetti 93/3, I-40129 Bologna, Italy*
[2]*Observatoire Astronomique de Strasbourg, Université de Strasbourg, CNRS UMR7550, F-67000 Strasbourg, France*
[3]*Max-Planck-Institut fur Astronomie, D-69117 Heidelberg, Germany*
[4]*Department of Physics, The Oskar Klein Centre for Cosmoparticle Physics, Stockholm University, AlbaNova, 114 21 Stockholm, Sweden*
[5]*Kapteyn Astronomical Institute, University of Groningen, PO Box 800, NL-9700 AV Groningen, The Netherlands*
[6]*INAF - Osservatorio Astrofisco di Arcetri, largo E. Fermi 5, I-50127 Firenze, Italy*

Accepted 2019 October 1. Received 2019 October 1; in original form 2019 July 30

ABSTRACT

We present radial velocities for five member stars of the recently discovered young (age $\simeq$ 100−150 Myr) stellar system Price-Whelan 1 (PW 1), which is located far away in the Galactic Halo (D$\simeq$ 29 kpc, Z$\simeq$ 15 kpc), and that is probably associated with the leading arm (LA) of the Magellanic Stream. We measure the systemic radial velocity of PW 1, $V_r = 275 \pm 10\,\mathrm{km\,s^{-1}}$, significantly larger than the velocity of the LA gas in the same direction. We re-discuss the main properties and the origin of this system in the light of these new observations, computing the orbit of the system and comparing its velocity with that of the H I in its surroundings. We show that the bulk of the gas at the velocity of the stars is more than 10 deg (5 kpc) away from PW 1 and the velocity difference between the gas and the stars becomes larger as gas closer to the stars is considered. We discuss the possibilities that (1) the parent gas cloud was dissolved by the interaction with the Galactic gas, and (2) that the parent cloud is the high-velocity cloud (HVC) 287.5+22.5 + 240, lagging behind the stellar system by $\simeq 25\,\mathrm{km\,s^{-1}}$ and $\simeq$10 deg $\simeq$ 5 kpc. This HVC, which is part of the LA, has metallicity similar to PW 1, displays a strong magnetic field that should help to stabilize the cloud against ram pressure, and shows traces of molecular hydrogen. We also show that the system is constituted of three distinct pieces that do not differ only by position in the sky but also by stellar content.

Key words: stars: kinematics and dynamics – open clusters and associations: individual: Price-Whelan 1 – galaxies: ISM – Magellanic Clouds.

1 INTRODUCTION

The second data release (DR2) of the Gaia space mission (see e.g. Brown et al. 2018; Lindgren et al. 2018, and references therein) has provided an unprecedented view of our own Galaxy, leading to the discovery of several new substructures and stellar systems of different provenance and nature (Cantat-Gaudin et al. 2018, 2019; Helmi et al. 2018; Malhan, Ibata & Martin 2018; Ibata, Malhan & Martin 2019; Torrealba et al. 2019, among others). While those studies used a variety of search techniques, an obvious and simple way to look for new stellar systems is to inspect density maps of blue stars. For instance, selecting stars with $(BP - RP)_0 < 0.0$ (see Evans et al. 2018, for a description of the Gaia DR2 photometric system) implies picking out mainly populations younger than $\simeq$ 500 Myr, tracing relatively recent star formation, and blue horizontal branch (BHB) stars, tracing old and metal-poor stars, while removing from the sample the vast majority of Galactic stars (Babusiaux et al. 2018).

A good example of the potential of this approach is provided by the map shown in Fig. 1. The map has been obtained, from Gaia DR2 data, from a first selection in observed colour[1] ($BP - RP$) < 0.5, in absolute Galactic latitude $|b| > 5.0$ deg, in `phot_bp_rp_excess_factor`, according to equation (C.2) by Lindgren et al. (2018), and keeping only sources with uncertainties in proper motions <1.0 mas yr^{-1} in both directions.[2] These selec-

★ E-mail: michele.bellazzini@inaf.it

[1]Not corrected for interstellar extinction.
[2]These selections on the `phot_bp_rp_excess_factor` and on the uncertainties in the proper motions are applied to all the samples extracted from Gaia DR2 that are used in this paper.

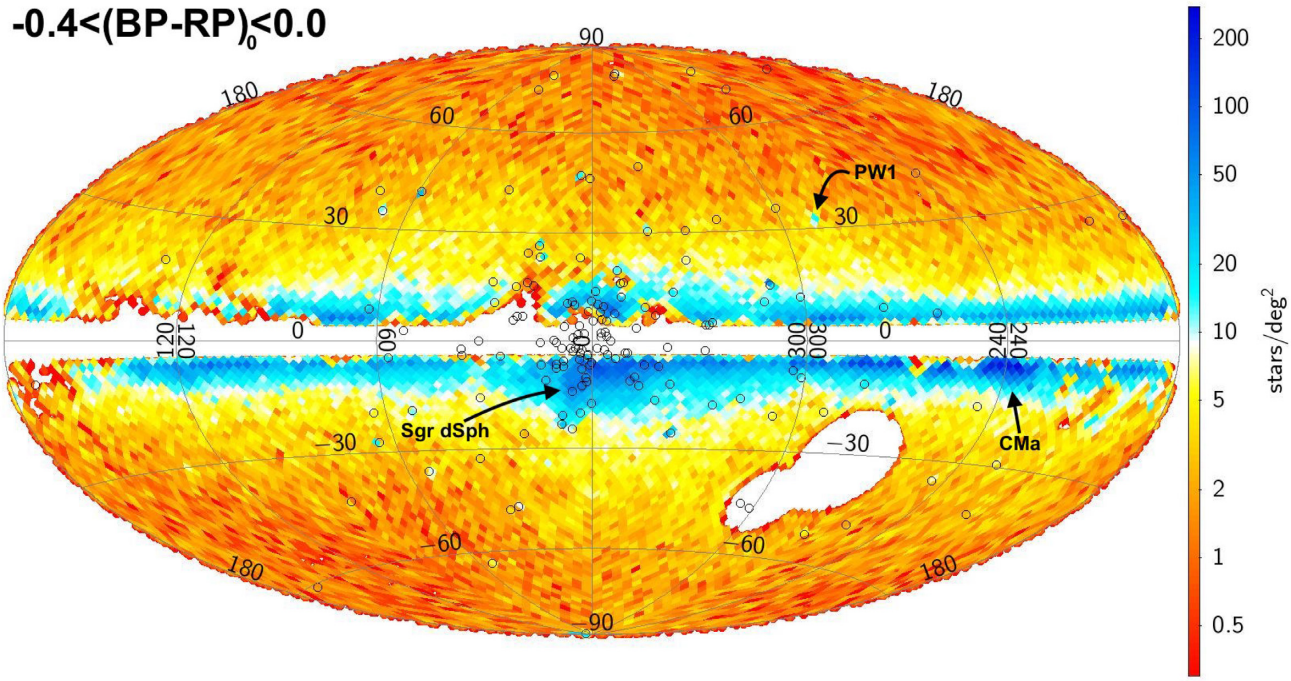

Figure 1. HEALPix density map (in logarithmic scale) of the blue stars with $|b| > 5.0$ deg from Gaia DR2 in Aitoff projection (Galactic coordinates). Two circular regions including the Magellanic Clouds have been excised. The open circles are the Galactic globular clusters from the 2010 version of the catalogue by Harris (1996). The position of Sgr dSph and the Canis Major overdensity are indicated and labelled.

tions lead to a sample of 2175 166 stars for which we obtain an estimate of the interstellar reddening $E(B-V)$ from the Schlegel, Finkbeiner & Davis (1998) maps, corrected with the calibration by Schlafly & Finkbeiner (2011). Then, we excised from the sample two wide circles around the position of the Large Magellanic Cloud (LMC) and Small Magellanic Cloud (SMC). The resulting map in Fig. 1 displays the 233 698 stars, from the sample described above, satisfying the condition $-0.4 < (BP-RP)_0 < 0.0$.

The most prominent structure in the map is the portion of the Galactic disc emerging at all longitudes just above our latitude limit $|b| = 5.0$ deg, where stars younger than $\simeq 500$ Myr are very abundant. Within the disc the most remarkable substructure is the Canis Major overdensity (Martin et al. 2004; Bellazzini et al. 2006; Momany et al. 2006), traced by its young main-sequence stars (Blue Plume; see Butler et al. 2007). On the other hand, the galactic Bulge is traced by its conspicuous population of BHB stars (see e.g. Montenegro et al. 2019, and references therein). The same happens for the Sagittarius dwarf spheroidal (Sgr dSph; Ibata, Gilmore & Irwin 1994; Majewski et al. 2003; Monaco et al. 2003), whose elongated shape is seen to plunge almost perpendicularly into the Galactic disc from the southern half of the Galaxy. Above and below the plane, several small-scale overdensities are clearly visible as the cyan-blue dots. Virtually, all of them, especially at high Galactic latitudes, are Galactic globular clusters (GGCs) that possess a significant BHB population, as demonstrated by their match with the positions of GGCs from the Harris (1996) catalogue (the black open circles). The only remarkable exception at $|b| \geq 15.0$ deg is the isolated cyan dot at (l,b) = (288.5 deg, 31.9 deg).

This small-scale overdensity turned out to have no known counterpart in catalogues of star clusters and/or nearby dwarf galaxies; it is an obvious clump also in the distribution of proper motions, and its colour–magnitude diagram (CMD) reveals the presence of a prominent main sequence typical of a young stellar cluster located at a large distance (>20 kpc), far in the Galactic Halo. While trying to understand the nature of this strikingly unusual object we realised that it had already been found, essentially with the same technique, by Price-Whelan et al. (2019; P19, hereafter), who reached conclusions very similar to those independently reached by us. In the following, we adopt their nomenclature, if not otherwise stated, starting from the name of the system: Price-Whelan 1 (PW 1).

According to the analysis by Price-Whelan et al. (2019), PW 1 is made up of a group ($M_* \simeq 1200$ M$_\odot$) of mildly metal-poor ([Fe/H] $\simeq -1.1$), 130 ± 6 Myr old stars, located at a distance of $D = 28.9 \pm 0.1$ kpc, with an interstellar extinction of $A_V = 0.33 \pm 0.02$. These values come from the statistical analysis of a deep CMD obtained from DECam images. The degeneracy between A_V, distance, and age leaves room for uncertainties on these parameters that may be significantly larger than those reported by P19. For instance, their estimate of the interstellar extinction towards PW 1 is $\simeq 0.1$ mag larger than what is obtained from the Schlegel et al. (1998) maps, corrected following Schlafly & Finkbeiner (2011). Still, the conclusion that PW 1 is the only stellar system younger than 1 Gyr known to inhabit the Galactic Halo, at a distance of about 30 kpc from us, is very robust (see next for further analysis and discussion). In the following, we will adopt the distance and metallicity estimates from P19, keeping in mind that the constraints on metallicity coming from the CMD are quite coarse. We also adopt the following reddening laws, provided by the online tool for the PARSEC stellar models [3] (see e.g. Bressan et al. 2012; Marigo et al. 2017): $A_G = 0.859E(B-V)$, $A_{BP} = 1.068E(B-V)$, $A_{RP} = 0.652E(B-V)$, for the Gaia DR2 photometry, and $A_g = 1.165E(B-V)$, $A_i = 0.676E(B-V)$, for PanSTARRS photometry (Chambers et al. 2016). Throughout the paper, we use only PARSEC

[3]CMD 3.3 http://stev.oapd.inaf.it/cgi-bin/cmd.

stellar models (Bressan et al. 2012) produced with the same tool, adopting the default configuration for the initial mass function and the bolometric corrections.

The spatial distribution of the stars in PW 1 does not show the radial symmetry typical of star clusters and dwarf galaxies. The stars are located in at least two main pieces, according to the nomenclature by P19: (1) a sparse main body containing most of the system's stars and (2) a minor but more compact component lying to the North of (1), separated by $\simeq 1.9$ deg $\simeq 1.0$ kpc. The internal motions are unresolved and P19 estimate a collective systemic motion in the plane of the sky of $\langle\mu_\alpha\rangle = -0.56 \pm 0.04$ mas yr^{-1} [4]and $\langle\mu_\delta\rangle = +0.47 \pm 0.02$ mas yr^{-1}. According to P19, this newly formed stellar system is likely slowly dissolving, as suggested by its sparse nature and odd morphology.

PW 1 is projected near the edge of one of the lanes (L II) of the so-called leading arm (LA; Putman et al. 1998), the arm of the Magellanic Stream (MS; see P19, Nidever et al. 2010; D'Onghia & Fox 2016, and references therein) that leads the Magellanic Clouds beyond the Galactic plane (see also Nidever, Majewski & Butler Burton 2008; Nidever et al. 2010; Venzmer, Kerp & Kalberla 2012). The very existence of a LA is interpreted as an evidence that Galactic tides had a major role in the origin of the MS (see e.g. D'Onghia & Fox 2016, for a thorough discussion of recent models for the formation of the MS). However, other hypotheses are also being considered, as, for instance, that the LA is formed from ram pressure stripping of a satellite of the Magellanic Clouds that is moving ahead of them (Hammer et al. 2015; Tepper-García et al. 2019; Wang et al. 2019)

Assuming values of the radial velocity matching those of the main features of the LA lying near PW 1, P19 show that the time since the system crossed the Galactic disc is similar to the age of its stars. Based on this finding, they suggest that the compression suffered by the gas in the MS while crossing the Galactic Disc lead to the small star formation episode that gave birth to PW 1 as a stellar system. Once born, the stars become kinematically decoupled from the gas (as they do not suffer from the drag exerted by Galactic gas), following a slightly different orbit. This hypothesis is very intriguing and, indeed, provides a reasonable explanation of the available observational data (including the similarity in the mean metallicity between PW 1 and L II; see e.g. P19 Lu et al. 1998; Wakker, Oosterloo & Putman 2002; Fox et al. 2018; Richter et al. 2018). If confirmed, it would have implications, e.g. providing the means for a direct estimate of the distance to the MS and to probe the gas density in the hot circum-Galactic corona (see P19 for a detailed discussion of the relationship of PW 1 with the MS and with the Magellanic system as a whole).

In this contribution, we present the first measurement of the heliocentric line-of-sight velocity (hereafter radial velocity, V_r) of PW 1, the only missing piece of the 3D motion of this object, allowing us to compute an orbit fully based on observational data. Moreover, we reconsider the main properties of the system, showing that it is likely made of three, partially independent pieces that differ not only in position but also in the mass range of their member stars.

2 THE STRUCTURE OF PW 1

In Fig. 2, we show a density map of stars from Gaia DR2 lying within 10 deg from the centre of PW 1, with a magnitude-dependent selection in parallax aimed at rejecting stars that are clearly at a lower distance with respect to PW 1,[5] and having proper motion within 1.0 mas yr^{-1} from the mean motion of the system. Note that 1.0 mas yr^{-1} corresponds to the typical uncertainty on proper motion for the faintest stars in our sample. Hence, while it may appear excessively relaxed, as it corresponds to $\simeq 137$ km s^{-1} at D = 28.9 kpc, it is conservatively set to minimize the loss of actual members, especially at faint magnitudes. This is particularly convenient, in this case, since the colour of PW 1 stars within the reach of Gaia DR2 is so blue that, when proper colour-cuts are adopted, the contamination from fore/background stars is negligible. In any case, all the results presented below are fully confirmed also when more stringent selection criteria are adopted (e.g. retaining only stars with proper motion within 0.5 mas yr^{-1} from the mean motion of PW 1).

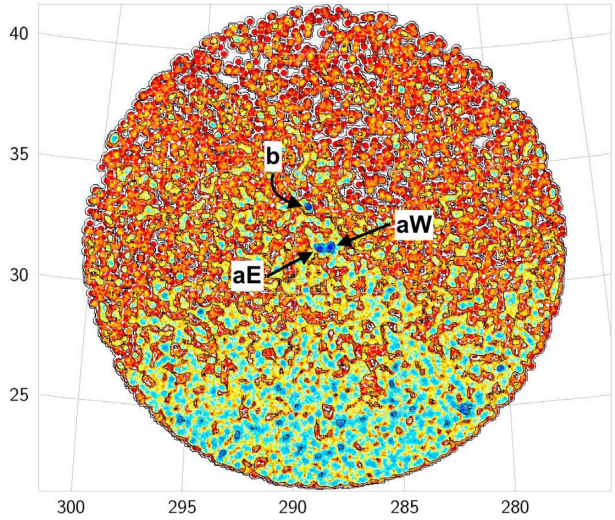

Figure 2. Density map (Galactic coordinates, logarithmic scale) of stars from Gaia DR2 in the region surrounding PW 1. Stars in this map are selected to have proper motion within 1.0 mas yr^{-1} from the mean motion of PW 1 and in parallax, to reject obvious nearby stars. The three components of the stellar system are indicated by the arrows and are labelled.

A large-scale density gradient is clearly visible in Fig. 2, as the Galactic disc, that dominates the surface density at $b \lesssim 30$ deg, gently disappears going towards the northern Galactic pole. PW 1 appears as three distinct compact density clumps. The main body 'a', at the centre of the map, is split into an eastern and a western component, aE and aW, hereafter. There is a hint of a diagonal band, emanating from the edge of the disc at (l,b)$\simeq$ (286 deg, 28 deg) and reaching (l,b)$\simeq$ (300 deg, 34 deg), that encloses PW 1. However, the stellar population and kinematics of the stars in this band are indistinguishable from those in the fore/background population surrounding PW 1, thus are likely not related to it.

The CMD of all the stars displayed in this map is shown in Fig. 3. The narrow blue main sequence of PW 1 is clearly evident, emerging at $(BP - RP)_0 \lesssim 0.1$ and $G_0 \lesssim 20.0$ from the typical Disc and Halo fore/background population (see P19 for the comparison with the CMD of control fields). In this plot, we also show the box by

[4]Where $\langle\mu_\alpha\rangle$ must be intended as $\langle\mu_\alpha\cos(\delta)\rangle$.

[5]In particular, we retain in the sample only stars having $|parallax| < 3.0(-16.4230 + 3.3644 * G_0 - 0.2273G_0^2 + 0.0051G_0^3)$. Note that proper motion and colour selected PW 1 members form a wedge-shaped distribution around $parallax = 0.0$ mas in the parallax versus G_0 plane. The wedge is narrow at bright magnitudes and widens towards the faint end, as the errors in parallax become larger with magnitude.

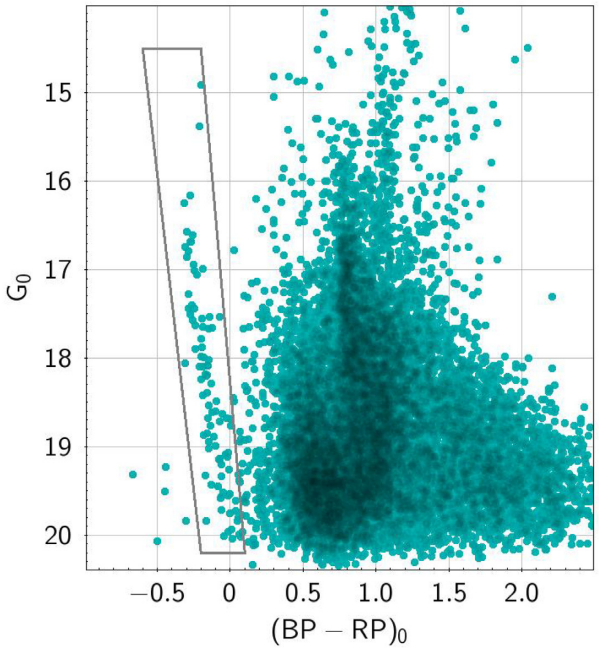

Figure 3. Colour–magnitude diagram of the same parallax and proper motion selected stellar sample shown in Fig. 2. The polygon shows the box in which we select the blue MS stars that are the characteristic population of PW 1.

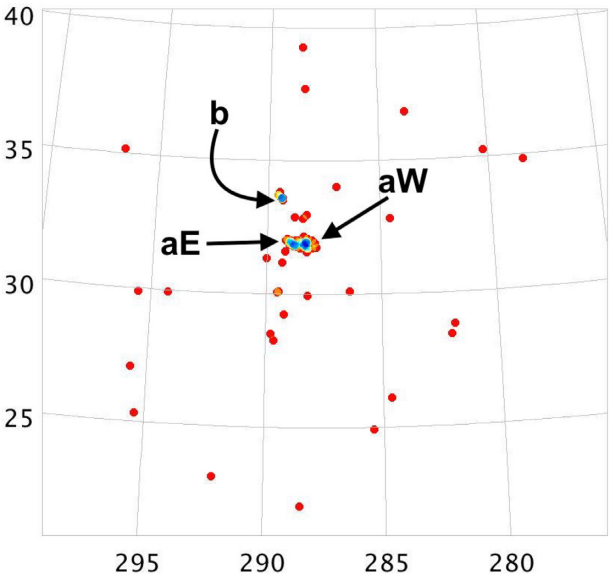

Figure 4. Density map (Galactic coordinates, logarithmic scale) of stars from the blue MS of PW 1, selected with the colour–magnitude box shown in Fig. 3.

which we further select the most likely members of PW 1 in colour and magnitude.

The stars selected with this box are displayed in Fig. 4. This further selection virtually removes everything not related to PW 1. It would be very interesting to follow-up spectroscopically all these stars since, if they are confirmed as members, they may be the best witnesses of the likely ongoing dissolution of the system. However, it would be surprising if the three stars lying in between aE + aW and b as well as those forming a kind of tail from the Southern edge

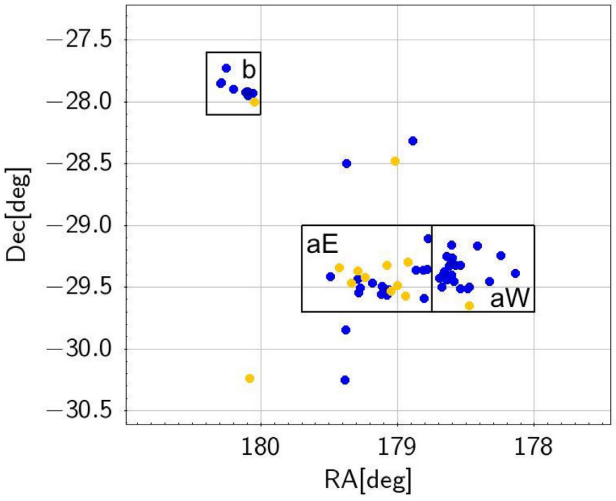

Figure 5. Zoomed version of Fig. 4 with boxes selecting stars in the three different pieces of PW 1. The yellow points mark stars having $G_0 < 17.1$.

of aE to $b \simeq -33$ deg, running nearly parallel to the $b = 180$ deg line were not (previous) members of the system. This map suggests that in the surrounding of PW 1 there are several blue MS stars likely related to it.

Fig. 5 provides a zoomed view of the same map, with the boxes we will adopt in the following to attribute stars to the various pieces of PW 1 (aE, aW, b). Triggered by the gap in the blue MS appearing at $G_0 = 17.1$ in the CMD of Fig. 3, here we plot in yellow the stars brighter than this limit. It is interesting to note that only one of these 15 bright stars is associated with aW, according to our selection, and this is the faintest one. aE and aW have the same total number of attributed members (25) but in aE nine of them are brighter than the apparent gap in the blue MS. One (of 25), as said is in aW and one (of 13) is in b. The remaining four bright stars are spread around the surrounding area. While its is hard to establish the statistical significance of this difference in the content of bright stars between aE and aW, Fig. 5 suggests that some degree of mass segregation is present within PW 1. We will discuss this feature in more detail in Section 4, next.

3 SPECTROSCOPIC OBSERVATIONS

We obtained optical spectra of five blue main-sequence stars from the central part of PW 1 selected as illustrated in Fig. 6. We choose two stars in aE (that we name aE1 and aE2, for brevity, hereafter; the open triangle and the square in Fig. 6), one from aW (aW1, asterisc), one from b (b1, the open pentagon) and one from the group of three stars lying between aE + aW and b (m1, the open star). The spectrum of a sixth star (belonging to aW) was also acquired but the signal to noise was too low to be useful, and we excluded it from further analysis. The main properties of these stars, including their Gaia DR2 identificative number, are reported in Table 1.

Observations were obtained during the nights of 2019 June 6 and 7, using the spectrograph EFOSC2 mounted at the 3.5 m New Technology Telescope [NTT, European Southern Observatory (ESO), La Silla]. We took one $t_{exp} = 900$ s spectrum per target using the Grism #19 with the `slit#0.5_red` slit, which is 0.5 arcsec but shifted with respect to the centre of the EFOSC2 field so as to allow observation at redder wavelengths. This set-up covers the spectral range 4441–5114 Å including the Mg'b' triplet, with a resolution $\lambda/\Delta\lambda \sim 6500$ at the wavelength of the H_β line. Observations of an

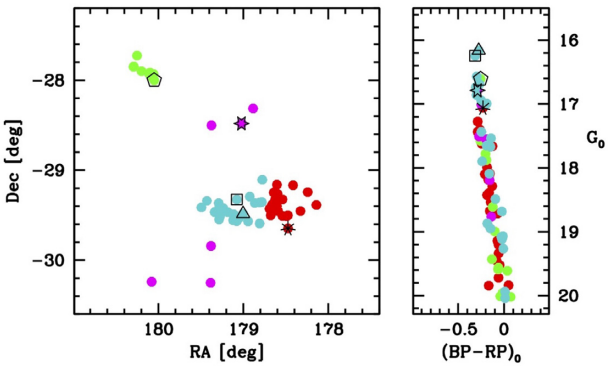

Figure 6. Positions of the spectroscopic targets in the sky map (left-hand panel) and in the CMD (right-hand panel) of PW 1. The targets are plotted with the same empty symbols in both panels. In both panels, the filled circles representing the stars of PW 1 are coloured according to the subsystem they belong to: aE (cyan), aW (red), and b (green). The stars that are likely members of the system but cannot be attributed to any of these pieces are plotted in magenta.

Argon–Helium arc-lamp were taken immediately after every target star before moving the telescope to minimize uncertainties from instrument flexure. All the spectra were reduced using standard IRAF procedures, including bias subtraction, flat-fielding, extraction, and wavelength calibration.

The final spectra are shown in Fig. 7. They all have similar signal-to-noise ratios (S/N∼6−7) but they differ in the strength of the only strong line that can be identified in all of them, that is H_β. Those having the strongest H_β, the two brightest and bluest stars aE1 and aE2, show also a hint of the neutral Helium line at 4921.9 Å. In the following analysis, we will use only H_β to estimate the radial velocity but we verified that the results obtained with the He I4921.9 line for these two stars are fully consistent with those obtained with H_β, albeit with a higher uncertainty.

We used IRAF/SPLOT to simultaneously fit the H_β absorption line with a Lorentzian profile, and the adjacent continuum with a straight line. The line centroid positions and the associated uncertainties were propagated into observed radial velocities and, finally, into heliocentric radial velocities by applying the heliocentric corrections computed with IRAF/RVCORR. The final uncertainties range from ∼10 to ∼30 km s^{-1}, depending on the strength of H_β in the considered spectrum. This precision is clearly not sufficient to resolve the internal motions of PW 1 but is more than sufficient to obtain the first measurement of its systemic radial velocity, a crucial piece of information that was still missing (P19).

The observed velocities ranges from $V_r = 253.1 \pm 25.9$ km s^{-1} to $V_r = 297.5 \pm 19.7$ km s^{-1}. The comparison with the predictions of the Besancon Galaxy Model (Robin et al. 2003)[6] towards this line of sight strongly suggests that none of the observed stars can be ascribed to the Milky Way galaxy. In particular, in a 1.0 deg^2 sample extracted from the model: (1) in the colour range of our target stars no model source has an heliocentric radial velocity larger than $V_r = 74.6$ km s^{-1}, and, (2) even considering stars of any colour, only 9 over 4770 have $G < 20.5$, $D > 20$ kpc, and $V_r > +250$ km s^{-1}, and all of them have negative values of μ_δ. We conclude that all our target stars are members of PW 1. Therefore, the star m1, though it does not reside in any of the three main pieces of PW 1, is physically associated with the system.

It may appear somehow intriguing that the two stars belonging to aE have very similar velocities (273.8 ± 11.1 km s^{-1} and 271.3 ± 13.0 km s^{-1}), and different from the stars from other subsystems of PW 1, but none of the observed differences is even marginally significant. For this reason, we consider the five stars as tracers of the same velocity distribution, and we consequently estimated the mean velocity and intrinsic velocity dispersion, following Martin et al. (2018). In practice, we infer the mean velocity $\langle V_r \rangle$ and the intrinsic velocity dispersion σ_i by assuming a Gaussian distribution of the five velocity data points and uniform priors and using the code JAGS[7] within the R environment.[8] The posterior PDF is shown in Fig. 8. The PDF of $\langle V_r \rangle$ is well behaved and Gaussian-like, hence, as our fiducial systemic velocity, we adopt the median of the PDF, with 1σ uncertainty given by the semidifference between the 84th and 16th percentiles: $\langle V_r \rangle = 275 \pm 10$ km s^{-1} (with $257 \leq \langle V_r \rangle \leq 294$ km s^{-1} at the 90 per cent confidence level). This corresponds to $\langle V_{LSR} \rangle = 272 \pm 10$ km s^{-1} in the Local Standard of Rest, and $V_{GSR} = 84 \pm 10$ km s^{-1} in the Galactic standard of rest, adopting the solar motion by Schönrich, Binney & Dehnen (2010) and the circular speed of the Sun from McMillan (2017). In a frame aligned with the Galactocentric cylindrical coordinates, with V_R pointing outwards from the Galactic centre, V_ϕ in the direction of rotation, and V_z pointing to the North Galactic pole, the 3D velocity vector is $(V_R, V_\phi, V_z) \simeq (-16, 8, 188)$ km s^{-1}. As expected, the intrinsic velocity dispersion is not resolved by our data. The mode of the PDF is $\sigma_i = 0.0$ km s^{-1}, with $\sigma_i \leq 32$ km s^{-1} at the 90 per cent confidence level.

It is very interesting to note that the derived radial velocity of PW 1 does not match the velocity of the nearby clouds of the LA. P19 identify three substructures as the possible gas counterparts of PW 1, at velocity $V_{LSR} \simeq 60$, 110, and 230 km s^{-1}, all significantly lower than our estimate $\langle V_{LSR} \rangle = 272 \pm 10$ km s^{-1}.

4 DISCUSSION

In Fig. 9, we compare the CMD of the three main pieces of PW 1 with a grid of four PARSEC isochrones, shifted to D = 28.9 kpc, with [M/H] = −1.1 and age ≃ 100, 160, 250, and 400 Myr. The comparison is performed using both Gaia DR2 and Pan-STARRS1 magnitudes, as a consistency check. Only colour-selected likely members are considered here. In the small portion of the CMD populated by PW 1 stars in Fig. 9, the isochrones are nearly vertical, thus providing poor constraints on the distance. This is the main reason why we rely on the distance (and metallicity) estimate of P19, obtained from a deeper and more complete CMD, reaching $G_0 \simeq g_0 \gtrsim 19.5$, where isochrones bend to the red, becoming more sensitive to this fundamental parameter.

The observed CMD is consistent with an age between 100 and 150 Myr, in agreement with the conclusions by P19. In this age regime and with such a sparse sample, the colour of the brightest stars is the most sensitive and reliable age indicator. In this respect, Fig. 9 suggests that with these assumptions on distance and metallicity, an age younger than 100 Myr is unlikely. It is also apparent from Fig. 9 that the CMDs of the three pieces are not identical. The most obvious difference is that virtually all the stars brighter than $G_0 = 17.1$ belong to aE, as anticipated in Section 2. If

[6] https://model.obs-besancon.fr

[7] http://mcmc-jags.sourceforge.net

[8] https://www.r-project.org

Table 1. Heliocentric radial velocities and other properties of the target stars.

Name	RA (deg)	Dec. (deg)	G_0 (mag)	BP_0 (mag)	RP_0 (mag)	$E(B-V)$ (mag)	V_r (km s^{-1})	Gaia DR2 id
aE1	179.00182010	−29.48336292	16.161	16.015	16.290	0.054	273.8 ± 11.1	3480054567924428032
aE2	179.07677448	−29.32545291	16.245	16.076	16.390	0.056	271.3 ± 13.0	3480064910205689088
b1	180.04853086	−28.00034847	16.608	16.481	16.736	0.064	297.5 ± 19.7	3486242378847130624
m1	179.02061045	−28.47964538	16.787	16.634	16.923	0.062	253.1 ± 25.9	3486167027940903296
aW1	178.47412626	−29.64657881	17.060	16.929	17.160	0.043	280.4 ± 28.4	3480036975738300800

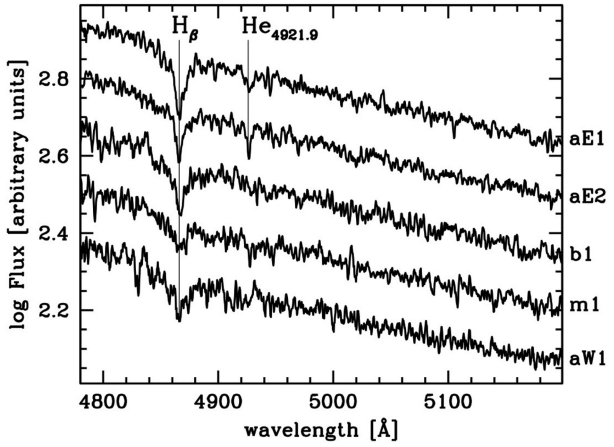

Figure 7. Spectra of the observed targets. Arbitrary shifts in log flux have been added to avoid overlapping the spectra within the panel. The only identifiable lines are marked and labelled.

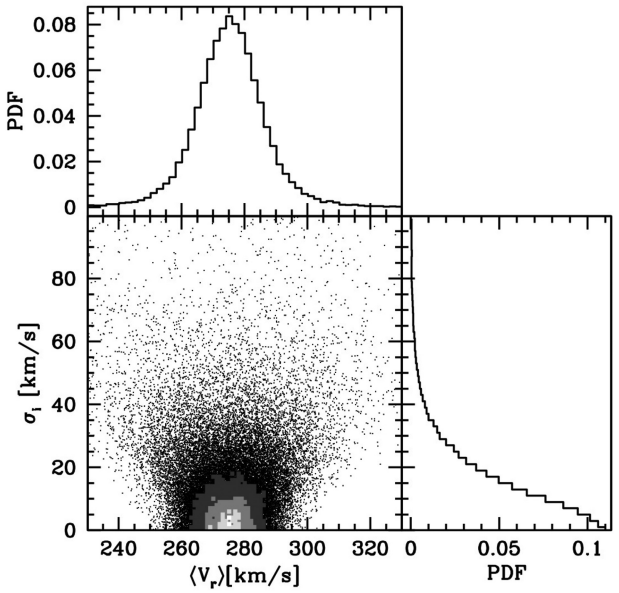

Figure 8. Joint PDF of the two-parameter Gaussian model (bottom left) and the marginalized PDF for the mean velocity (top) and the intrinsic velocity dispersion (right).

the distance, age, and metallicity assumptions we made are correct, and we are dealing with genuine single stars, virtually all the stars with $M > 3.8\,M_\odot$, up to $M \simeq 4.5\,M_\odot$, are segregated into aE. This may be merely due to small number statistics, but also to slight differences in age, binary content, and/or distance between the various pieces. For example, this correlation between position

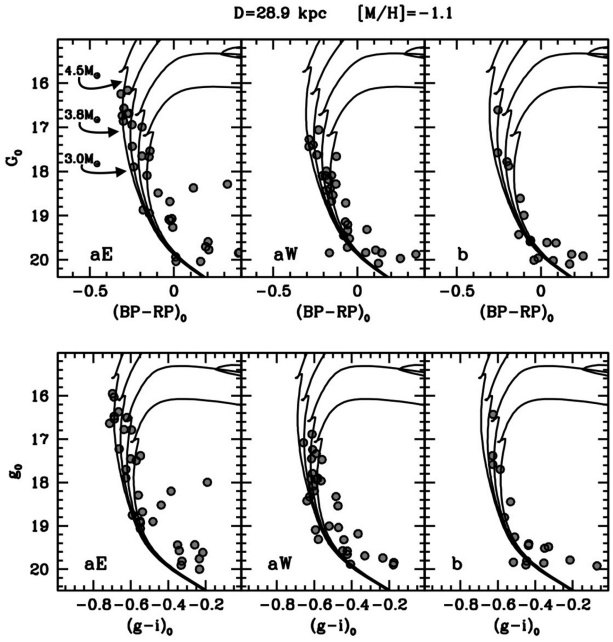

Figure 9. CMDs of the aE, aW and b subsystems (left-hand, central, and right-hand panels, respectively) from Gaia DR2 (upper row of panels) and PanSTARRS1 (lower row of panels) photometry. On each CMD, we overplotted four isochrones at metallicity [M/H] = −1.1, shifted to the distance of PW 1, with age ≃ 100, 160, 250, and 400 Myr, from left to right, from the PARSEC set. In the upper left-hand corner we indicated the initial stellar masses corresponding to G_0 =16.0, 17.1, and 18.0 on the age = 100 Myr isochrone.

and stellar content may hint at a slightly different epoch of formation in different fragments of the parent gas cloud of PW 1. In any case it provides further support, in addition to the density field, to the idea that PW 1 is constituted by three distinct pieces.

A rough estimate of the stellar mass of the system can be obtained by fitting a theoretical model to the observed luminosity function (LF), thus allowing a sound extrapolation to the stars that went undetected because they are fainter than the limiting magnitude of our sample. To do this, we adopt a PARSEC model with age = 100 Myr and [M/H] = −1.1, shifted to D = 28.9 kpc, as above. To compare the observed and the model LFs in a fully homogeneous way, including the same binning, the theoretical LF was derived from a synthetic population of 12 000 $M_\odot$ with the adopted age and metallicity, obtained with CMD 3.3.

To obtain the best-fitting normalization between the observed and theoretical LFs, that corresponds to a total stellar mass, we minimize χ^2 in the range $G_0 < 18.5$, as at fainter magnitudes the effect of incompleteness is apparent. In Fig. 10, we show the best fit to the LF of all the MS stars selected as possible current or former members of PW 1 (shown in Fig. 4), leading to $M_{*,\,tot} \simeq 1700\,M_\odot$. We repeated

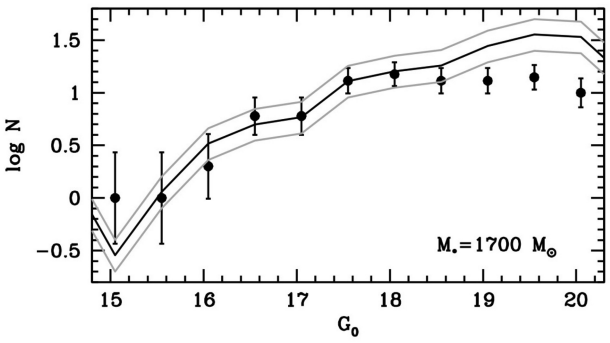

Figure 10. Luminosity Function (LF) of all the PM-selected, parallax-selected, and colour-selected possible members of PW 1 shown in Fig. 4. The black line is the theoretical LF from an age = 100 Myr, [M/H] = −1.1 PARSEC model that best fits the observations in the range $G_0 < 18.5$, corresponding to $M_* \simeq 1700\,M_\odot$. The grey curves are the theoretical LF adopting different normalization factors, corresponding to $M_* = 2000\,M_\odot$ (upper curve) and to $M_* = 1000\,M_\odot$ (lower curve).

Table 2. Structural parameters of PW 1 and its substructures.

Name	RA_0^a (deg)	$Dec._0$ (deg)	M_*^b ($M_\odot$)	M_V^c (mag)	r_{50}^d (arcmin)	R_{50}^e (pc)
PW 1 (all)	–	–	≤1716	≥−5.5	–	–
aE + aW	178.8	−29.4	1056	−4.9	17.9	150
aE	179.1	−29.5	684	−4.5	14.1	118
aW	178.6	−29.3	516	−4.2	12.9	108
b	180.1	−27.9	192	−3.1	3.1	26

[a] RA_0, $Dec._0$ are the coordinates of the density peak of the subsystem, except for aE + aW, for which we adopted the position by P19.
[b] Best-fitting values from fitting the LF as in Fig. 10.
[c] Adopting $M/L_V = 0.13$, from the age = 100 Myr and [M/H] = −1.1 model.
[d] Angular radius enclosing half of the members.
[e] Physical radius enclosing half of the members, adopting D = 28.9 kpc.

the exercise for all the various pieces of PW 1 and we report the exact values of the best-fitting normalizations in Table 2, to be taken, as said above, with due caution, given all the systematic uncertainties that can affect the comparison. Reassuringly, for aE + aW we obtain $M_* \simeq 1100\,M_\odot$, in good agreement with the results of P19 for the same part of the system ($M_* = 1200\,M_\odot$). From the same model used to fit the LF, we can obtain the mass-to-light ratio in the Johnson-Cousin *V* band ($M/L_V = 0.13$), and, consequently, we convert the mass estimates into estimates of M_V, also reported in Table 2.

Following Cantat-Gaudin et al. (2018), as a size indicator we computed r_{50} (in arcmin, R_{50} in parsec), which is the radius enclosing half of the members of each subsystem, adopting the memberships illustrated in Fig. 5. This choice has two desirable features: first, r_{50} is the best proxy for the half-light radius that we can obtain from our data; secondly it allows a direct and fully homogeneous comparison with the 1229 Galactic open clusters for which Cantat-Gaudin et al. (2018) provide an estimate of the same parameter. Adopting their modal distance (D_{mod}), the open clusters of Cantat-Gaudin et al. (2018) have $0.2 < R_{50} < 15.2$ pc, with a median of 2.75 pc and 90 per cent of the sample having $R_{50} \leq 5.2$ pc. It is very interesting to note that the only piece of PW 1 that has a size comparable with that of star clusters is b ($R_{50} = 26$ pc). On the other hand, aE, aW, and the two taken together have $R_{50} \sim 100-150$ pc, in the range spanned by dwarf galaxies of similar luminosity (see e.g. McConnachie 2012; Torrealba et al. 2019). As already noted by P19, PW 1 has the stellar mass and stellar population of an open cluster but the size of a dwarf galaxy, suggesting that we are seeing the system while it is dissolving into the halo, being not bound by self-gravity. It is important to stress that these estimates of r_{50} were only intended to provide an idea of the typical size of the fragments. Given their irregular morphology and the lack of obvious centres of symmetry, a characteristic radius is clearly not fully adequate to describe the structure of PW 1 pieces. In particular, aE is nearly filamentary, with a shell morphology that is observed also in other places where star formation is occurring, triggered by interactions (e.g. Martinez-Delgado et al. 2019).

If PW 1 is indeed the product of a small recent episode of star formation that occurred within a cold gas cloud, associated or not associated with the MS (see next) and likely triggered by interaction with Galactic gas, an interesting similarity, albeit at a smaller scale, can be noted with SECCO 1 (see Bellazzini et al. 2018, and references therein). This is a low-mass ($M_* = 10^5\,M_\odot$) star-forming system (with no detection of stars older than ∼50 Myr) located in the outskirts of the Virgo cluster of galaxies, which is the possible prototype of a new class of stellar systems that are born in isolated H I clouds kept together by the external pressure of the surrounding hot gas (Sand et al. 2017; Bellazzini et al. 2018). SECCO 1 is fragmented in two pieces, each one with size of a few hundreds of pc, and will probably fragment into smaller pieces in the near future. While the largest subsystem of SECCO 1 (main body, MB) lies within an H I cloud of $\sim 10^7\,M_\odot$, the smallest fragment (secondary body, SB) has no cold gas detected in coincidence with the stellar body, but it is likely associated with a $M \simeq 10^6\,M_\odot$ cloudlet having the same velocity but offset by ∼2.5 kpc, in projection, with respect to the stars. We will see next that this is reminiscent of the configuration of PW 1 with respect to a nearby isolated small gas cloud.

4.1 The orbit of PW 1

Adopting the position and mean proper motion from P19 and the radial velocity derived here, we integrated the orbit of PW 1 backward for 1.0 Gyr using GravPot16 (Fernández-Trincado et al. 2017).[9] This tool adopts the Galactic potential of the Besancon Galactic Model (Robin et al. 2003),[10] including a rotating bar and an isothermal dark matter halo, and it has been recently used, within the Gaia Collaboration, to compute the orbits of many Galactic satellites (Helmi et al. 2018). We independently checked the results with other orbit integrators adopting different models of the Galactic potential, and we verified that the main results presented in this section are robust to these systematic uncertainties.

The path of the newly computed orbit during the last 250 Myr is displayed in Fig. 11. The orbit is confined within $\lesssim 1.5$ kpc of the *Y*–*Z* plane, with an inclination of 87.6 deg to the Galactic Plane. The perigalactic and apogalactic distances are $R_{peri} = 13.8$ kpc and $R_{apo} = 32.8$ kpc, eccentricity $e = 0.41$, and period P = 0.47 Gyr. The crossing of the Galactic disc occurs $t_c = 70$ Myr ago. To explore the effect of the uncertainties of the initial conditions on the estimate of t_c, we repeated the integration over a coarse grid where, at each node, one of the relevant parameters ($\langle\mu_\alpha\rangle$, $\langle\mu_\delta\rangle$, $\langle V_r\rangle$, and the distance) was changed by $\pm 1\sigma$ and all the others were kept fixed at their best-estimated value. To be conservative, for the distance we adopted a

[9] https://fernandez-trincado.github.io/GravPot16/index.html
[10] https://model.obs-besancon.fr

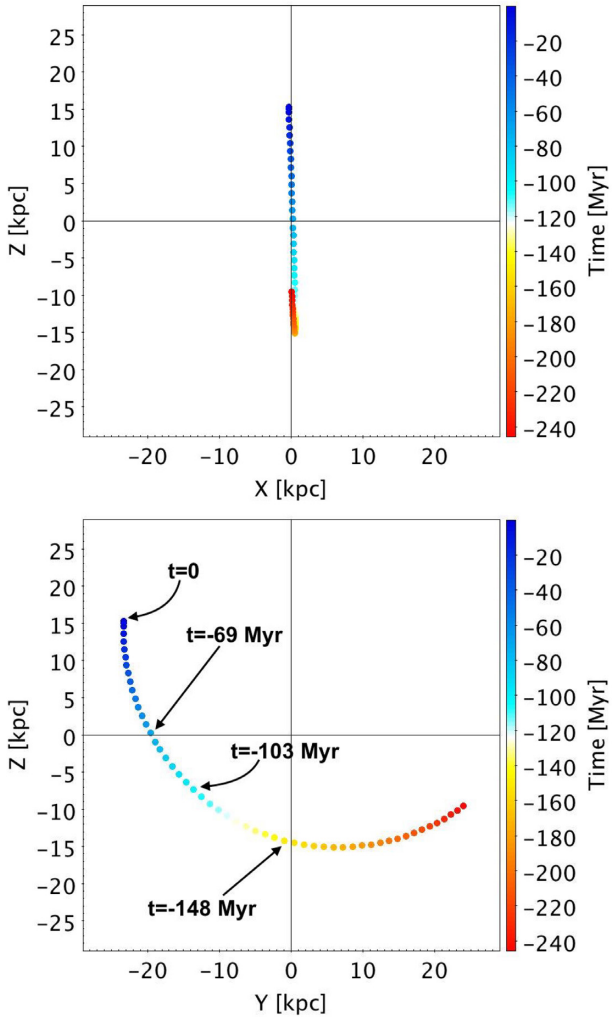

Figure 11. Orbit of PW 1 during the last 250 Myr projected into the *X*–*Z* (upper panel) and *Y*–*Z* (lower panel) planes of a right-handed Galactocentric Cartesian coordinate system. In this system, the Sun is located at (X,Y,Z) = −8.1,0,0). The epoch of each point in the orbit is colour coded with the look-back time in Myr. In the lower panel, we have labelled the points corresponding to a few remarkable epochs: the present day, corresponding to the current position of PW 1, the first computed position after the crossing of the Galactic Plane, 69 Myr ago, and the position of the system at the computed points nearest to 100 and 150 Myr ago.

1σ uncertainty of 1.0 kpc, i.e. 10 times larger than that reported by PW1. Moreover, since the distance and the radial velocity are the parameters bearing the largest uncertainties and having the highest impact on t_c, we included in the grid also all the combinations implying simultaneous 1σ variations of both parameters. In total, we explore 12 sets of initial conditions in addition to the best ones and we found that the impact on the predicted epoch of disc crossing is remarkably small, $68 \leq t_c \leq 74$ Myr. These results are summarized in Table 3.

Compared at face value with the age of the system derived above (100–150 Myr), $t_c \simeq 70^{+4}_{-2}$ Myr would imply that the star formation was ignited before the disc crossing, when PW 1 was ∼7−14 kpc below the plane. However, given the significant uncertainties that are still involved into this comparison, in our view, the similarity of the two time-scales remains strongly suggestive of a connection between the crossing of the disc and the onset of star formation

Table 3. Times since the crossing of the Galactic Plane as a function of initial conditions for orbit integration.

D (kpc)	$\langle\mu_\alpha\rangle$ (mas yr^{-1})	$\langle\mu_\delta\rangle$ (mas yr^{-1})	$\langle V_r\rangle$ (km s^{-1})	t_c (Myr)
28.9	−0.56	0.47	275	70.1
27.9	−0.56	0.47	265	69.6
27.9	−0.56	0.47	275	68.0
27.9	−0.56	0.47	285	68.6
28.9	−0.52	0.47	275	69.8
28.9	−0.56	0.47	265	71.8
28.9	−0.56	0.47	285	68.6
28.9	−0.56	0.49	275	69.5
28.9	−0.56	0.45	275	70.8
28.9	−0.60	0.47	275	70.5
29.9	−0.56	0.47	265	73.9
29.9	−0.56	0.47	275	72.2
29.9	−0.56	0.47	285	70.7

*Notes.*The crossing time has been derived by linear unterpolation between the two computed points of the orbit bracketing Z = 0.0 kpc. The first row corresponds to the best-estimate initial conditions.

in PW 1. Presumably, future data releases of Gaia and spectroscopic estimates of the metal content will significantly reduce the uncertainty in the orbit (distance and 3D motion) and in the age of the system, allowing us to establish if these key events have been simultaneous or not.

4.2 The parent gas cloud of PW 1

PW 1 is a very special case among the stellar systems orbiting the Milky Way. In particular, it is the only known object lying so far from the Galactic Disc (Z≃ 15 kpc) that is made only of young stars (age $\lesssim$ 150 Myr), calling for recent association with some H I structure/cloud. Neutral hydrogen is also relatively rare in these remote regions of the Galactic Halo, hence the proximity of PW 1 to an arm of the main H I structure within the Halo, the MS, is strongly suggestive of a physical association. Small-scale episodes of recent star formation likely associated with the interactions between the two Magellanic Clouds and the Milky Way are known to occur, e.g. in the Magellanic Bridge, in the outskirts of the SMC (Skowron et al. 2014; Martinez-Delgado et al. 2019), and possibly also in the LA (Casetti-Dinescu et al. 2014)[11]

P19 suggested that the crossing of the Galactic Disc by the head of the MS LA triggered the star formation episode that produced PW 1. Then, the newly formed stars decoupled from the parent H I cloud, as they are free from the drag exerted on the moving cloud by the Galactic gas in the disc and in the corona. If this were to be the case, a velocity and position lag between PW 1 and the parent gas structure may be expected. However, since both the star formation event and the crossing of the disc are recent (70–150 Myr), it may be expected that the lag should be small, and the nearest H I in projection should also display the smallest velocity lag.

In Fig. 12, we show a series H I channel maps in the surroundings

[11]However, Zhang et al. (2019) showed that the orbital parameters of most of the Casetti-Dinescu et al. stars are not compatible with an association with the LA. Moreover, we verified that none of the stars followed up by Zhang et al. (2019) are compatible with the orbit of PW 1. In particular, all of them have $Z_{max} < 10.0$ kpc, to be compared to $Z_{max} = 32.6$ kpc of our fiducial orbit of PW 1 and to its current height above the Galactic plane, $Z = 15.2$ kpc.

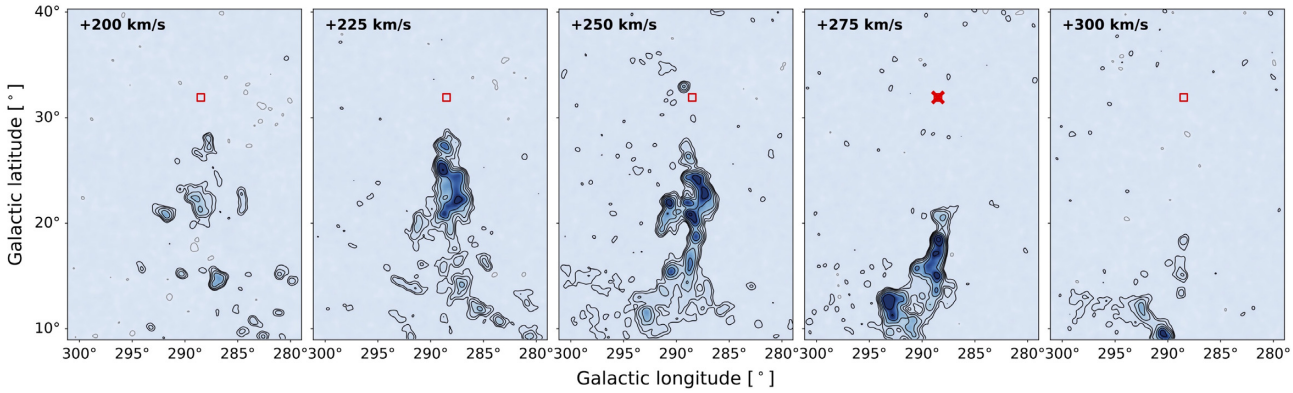

Figure 12. H I density fields from HI4PI mapping the region of the edge of the MS Leading Arm near PW 1, in five radial velocity channels bracketing the velocity of the stellar system. The adopted spatial resolution is 0.54 deg FWHM. The contours correspond to brightness temperatures ranging from $T_B = 0.035$ K (corresponding to 3 × the rms noise), to 2.24 K, increasing in steps of factor of 2. An empty red box marks the position of PW 1 in all the maps, an additional red cross highlights the map of the $V_r = +275\,km\,s^{-1}$ channel, corresponding to the velocity of PW 1.

of PW 1, and focused on the MS LA, from the all-sky HI4PI survey (Ben Bekhti et al. 2016). This figure shows that (1) indeed, there is no H I with $T_B \geq 0.035$ K that coincides in position with PW 1, and (2) the H I velocity trend is in the opposite sense with respect to that envisaged above. As the radial velocity of the gas increases from $+200\,km\,s^{-1}$ to reach the velocity of the stars ($+275\,km\,s^{-1}$) and beyond, the mean latitude of the gas distribution decreases, moving away from the position of PW 1 towards the Galactic Disc. While the Northern edge of the gas distribution at $V_r = 200{-}225\,km\,s^{-1}$ is about ∼4 deg apart from the stellar system, corresponding to ∼2 kpc at D = 28.9 kpc, at $V_r = 275\,km\,s^{-1}$ the gas is ∼10 deg apart, corresponding to ∼5 kpc.[12] The described trend is in good agreement with the overall gradient observed along the LA by Venzmer et al. (2012), with the gas decelerating from $V_{GSR} = 84.2\,km\,s^{-1}$, at the position of the LMC, to about $V_{GSR} = 6\,km\,s^{-1}$ in the proximity of PW 1, that, instead, has $V_{GSR} = 84 \pm 10\,km\,s^{-1}$.

Realistic hydrodynamical modelling of the complex interaction between the LA and the Galactic gaseous disc and corona are required to explore in detail the evolutionary paths that may have led to the observed configuration. Next, we briefly discuss two possible scenarios that are broadly compatible with the available data.

4.2.1 *Dissolution of the parent cloud*

The lack of a good match with known structures may suggest that the parent cloud of PW 1 is not detectable in H I anymore, having already disappeared. Indeed, fragmentation is observed to occur in the MS (Nidever et al. 2008, 2010; For et al. 2014, and references therein), especially at the edge of the LA, near PW 1 (Venzmer et al. 2012; For et al. 2014; D'Onghia & Fox 2016), and low-mass clouds of cold gas ($M \leq 10^5\,M_\odot$) may be dissolved on short time-scales ($\lesssim$ 100–200 Myr, depending on the initial mass) by the interaction with the circumgalactic medium (see e.g. Heitsch & Putman 2009; Armillotta et al. 2017, and references therein). In particular, Tepper-García & Bland-Hawthorn (2018), based on the results of a set of hydrodynamical simulations of the evolution of the Smith cloud (Smith 1963), concluded that a massive ($M \gtrsim 10^8\,M_\odot$), dark-matter free high-velocity cloud (HVC; Wakker & van Woerden 1997) crossing the Galactic disc with Galactocentric distance and velocity similar to PW 1, cannot survive the transit.

The signatures of ongoing ram pressure stripping on LA structures have been noted and discussed by Venzmer et al. (2012). In this case, the feedback from star formation (supernovae) could have contributed to blow the residual gas away from the stellar system. In this context, it is interesting to note the compact cloudlet at (l,b)≃ (289.4 deg, 32.9 deg) in the $V_r = 250\,km\,s^{-1}$ snapshot of Fig. 12. This is the known H I structure nearest to PW 1, in projection (just ≃ 1.3 deg, corresponding to ≃ 0.7 kpc), with a velocity difference that is relatively modest ($21.5\,km\,s^{-1}$, in the Galactic standard of rest). At the distance of PW 1, its integrated flux corresponds to an H I mass $M_{HI} \simeq 3000 \pm 300\,M_\odot$, about twice the total stellar mass of PW 1, hence it can be a plausible candidate for the gaseous residual of the formation of PW 1.

4.2.2 *Flying away from HVC 287.5+22.5 + 240*

On the other hand, Fig. 12 may be seen, from right to left, as depicting the progressive deceleration of the gas cloud that gave origin to PW 1 as it penetrates in the northern galactic hemisphere after having crossed the disc, while PW 1 is flying away, free of any drag from the Galactic gas. Note that this may happen independently of the actual origin of the LA (gas tidally + ram pressure stripped from the SMC or trailing gas from an LMC/SMC satellite running ahead of the MCs, as suggested, e.g. by Tepper-García et al. 2019). In this scenario, the clouds nearest to PW 1 are those that have suffered the highest degree of deceleration, thus showing a larger velocity lag with respect to the stellar system.

In this context, it is interesting to note that the gas structure that dominates the map in the central panel of Fig. 12, at $V_r = +250\,km\,s^{-1}$ (corresponding to $V_{LSR} \simeq 245\,km\,s^{-1}$), is a well known and thoroughly studied HVC: HVC 287.5+22.5 + 240 (also known as WW 187; see Wakker et al. 2002, and references therein). In particular, detailed chemical abundance analyses have been performed by various authors, from UV spectra of the background Seyfert galaxy NGC 3783 (Lu et al. 1998; Wakker et al. 2002; Fox et al. 2018; Richter et al. 2018). The abundance pattern is found to match very closely that of the SMC, thus pointing to an origin from an episode of gas stripping from this galaxy (Richter et al. 2018, their fig. 6, in particular).

[12]Note that even if the radial velocity is the same, the 10 deg distance in the sky implies also a difference of $\sim 20\,km\,s^{-1}$ in V_{GSR}.

It is very interesting to note that the abundance of sulphur in HVC 287.5+22.5 + 240, an element that is virtually immune from dust depletion, is $[S/H] \simeq -0.6$ (Lu et al. 1998; Wakker et al. 2002; Richter et al. 2018). Adopting $[S/Fe] \simeq +0.6$ for SMC stars, according to Russel & Dopita (1992) and following Lu et al. (1998), and assuming a common original composition for the HVC and the SMC, $[Fe/H] \simeq -1.2$ is obtained for HVC 287.5+22.5 + 240, remarkably similar to the available estimate for PW 1 ($[Fe/H] = -1.1$).

Moreover, McClure-Griffiths et al. (2010) found that HVC 287.5+22.5 + 240 is the only case, among the 27 HVCs/gas complexes analysed by these authors, displaying a strong and coherent magnetic field. According to McClure-Griffiths et al. (2010), the observed field is consistent to that required to dynamically stabilize the cloud against ram pressure. This factor may have played a major role to let HVC 287.5+22.5 + 240 survive the crossing of the Galactic disc, providing a natural way out from the conclusions by Tepper-García & Bland-Hawthorn (2018). Finally, molecular hydrogen, typically conducive to star formation, has been detected in this HVC (Sembach et al. 2001; Richter et al. 2018).

These evidences provide significant support to the hypothesis that HVC 287.5+22.5 + 240 is the parent cloud of PW 1, within the interpretative scheme originally advanced by P19 for the origin of PW 1.

5 SUMMARY AND CONCLUSIONS

We have acquired EFOSC2@NTT medium-resolution spectra of five members of the recently discovered young stellar system Price-Whelan 1, lying at D$\simeq$ 29 kpc from us, at a height of $\simeq$ 15 kpc from the Galactic plane. These spectra allowed us to obtain the first measurement of its systemic radial velocity $V_r = 275 \pm 10\,\mathrm{km\,s^{-1}}$. Having at disposal all the three components of the spatial velocity of PW 1, we computed its orbit within a realistic Galactic potential. According to the newly derived orbit, the system crossed the Galactic plane 70 Myr ago, a time-scale comparable with its estimated age (100–150 Myr).

The proximity with the LA of the MS lead to the hypothesis that PW 1 formed at the edge of this huge H I structure (P19). However, its radial velocity is significantly different from the gas in the nearest edge of the LA. We briefly discuss the possibility that the parent cloud of PW 1 has already dissolved into the Galactic corona and also the possible identification of the nearby HVC, HVC 287.5+22.5 + 240 as the birthplace of PW 1.

We show that PW 1 is made of three main pieces (plus additional likely members dispersed in the surroundings), and we provide estimates of the stellar mass, absolute integrated V magnitude, and a proxy of the half-light radius for each of them. We provide also evidence that the stellar content of the three pieces is not exactly the same, the brightest / most massive stars residing almost exclusively in the aE subsystem.

A direct spectroscopic metallicity estimate is probably the most relevant piece of information that is currently missing to constrain the nature and the origin of this very unusual stellar system, as it would strongly mitigate the effects of the age/distance/metallicity degeneracy that now is leaving room to significant systematic uncertainties in these key parameters. Resolving the internal kinematics would also be very useful to finally establish if PW 1 is indeed dissolving, also constraining the relevant time-scales for this process.

ACKNOWLEDGEMENTS

We are grateful to an anonymous referee for providing very useful suggestions that significantly improved this paper. MB is grateful to A. Sollima, F. Fraternali, A. Bragaglia, D. Romano, and A. Mucciarelli for useful suggestions and discussion, and to J.G. Fernández-Trincado for his precious help with GalPot16.

Based on observations collected at the European Southern Observatory under ESO programme 103.B-0568(A).

This project has received funding from the European Research Council (ERC) under the European Union's Horizon 2020 research and innovation programme (grant no. 834148)

This work has used data from the European Space Agency (ESA) mission Gaia (http://www.cosmos.esa.int/gaia), processed by the Gaia Data Processing and Analysis Consortium (DPAC, http://www.cosmos.esa.int/web/gaia/dpac/consortium). Funding for the DPAC has been provided by national institutions, in particular the institutions participating in the Gaia Multilateral Agreement.

This work has used data from the Pan-STARRS1 Surveys (PS1). The PS1 and the PS1 public science archive have been made possible through contributions by the Institute for Astronomy, the University of Hawaii, the Pan-STARRS Project Office, the Max-Planck Society and its participating institutes, the Max Planck Institute for Astronomy, Heidelberg, and the Max Planck Institute for Extraterrestrial Physics, Garching, The Johns Hopkins University, Durham University, the University of Edinburgh, the Queen's University Belfast, the Harvard-Smithsonian Centre for Astrophysics, the Las Cumbres Observatory Global Telescope Network Incorporated, the National Central University of Taiwan, the Space Telescope Science Institute, the National Aeronautics and Space Administration under grant no. NNX08AR22G issued through the Planetary Science Division of the NASA Science Mission Directorate, the National Science Foundation grant no. AST-1238877, the University of Maryland, Eotvos Lorand University (ELTE), the Los Alamos National Laboratory, and the Gordon and Betty Moore Foundation.

Most of the analysis presented in this paper has been performed with TOPCAT (Taylor 2005). This research has used the GravPot16 software, a community-developed core under the git version-control system on GitHub. This research has used the SIMBAD data base, operated at CDS, Strasbourg, France. This research has used the NASA/IPAC Extragalactic Data base, which is operated by the Jet Propulsion Laboratory, California Institute of Technology, under contract with the National Aeronautics and Space Administration. This research has used NASA's Astrophysics Data System.

REFERENCES

Armillotta L., Fraternali F., Werk J. K., Prochaska J. X., Marinacci F., 2017, MNRAS, 470, 114
Bellazzini M., Ibata R., Martin N., Lewis G. F., Conn B., Irwin M. J., 2006, MNRAS, 366, 865
Bellazzini M. et al., 2018, MNRAS, 476, 4565
Ben Bekhti N. et al., 2016, A&A, 594, A116
Bressan A., Marigo P., Girardi L., Salasnich B., Dal Cero C., Rubele S., Nanni A., 2012, MNRAS, 427, 127
Butler D. J., Martínez-Delgado D., Rix H.-W., Peñarrubia J., de Jong J. T. A., 2007, AJ, 133, 2274
Cantat-Gaudin T. et al., 2018, A&A, 618, A93
Cantat-Gaudin T. et al., 2019, A&A, 624, A126
Casetti-Dinescu D. I., Moni Bidin C., Girardi R. M. et al., 2014, ApJ, 784, L37
Chambers K. C. et al., 2016, preprint (arXiv:1612.05560)

D'Onghia E., Fox A. J., 2016, ARA&A, 54, 363
Evans D. W. et al., 2018, A&A, 616, A4
Fernández-Trincado J. G., Robin A. C., Moreno E., Pérez-Villegas A., Pichardo B., 2017, in Reylé C. et al., eds, SF2A-, 2017: Proceedings of the Annual meeting of the French Society of Astronomy and Astrophysics. p. 193, preprint (arXive:1708.05742)
For B.-Q., Staveley-Smith L., Matthews D., McClure-Griffiths N. M., 2014, ApJ, 792, 43
Fox A. J. et al., 2018, ApJ, 854, 142
Gaia Collaboration, 2018, A&A, 616, A10
Gaia Collaboration, 2018, A&A, 616, A1
Gaia Collaboration, 2018, A&A, 616, A12
Hammer F., Yang Y. B., Flore H., Puech M., Fouquet S., 2015, ApJ, 813, 110
Harris W. E., 1996, AJ, 112, 1487
Heitsch F., Putman M. E., 2009, ApJ, 698, 1485
Helmi A., Babusiaux C., Koppelman H. H., Massari D., Veljanoski J., Brown A. G. A., 2018, Nature, 563, 85
Ibata R. A., Gilmore G., Irwin M. J., 1994, Nature, 370, 194
Ibata R. A., Malhan K., Martin N. F., 2019, ApJ, 872, 152
Lindgren L. et al., 2018, A&A, 616, A2
Lu L., Savage B. D., Sembach K. R., Wakker B. P., Sargent W. L. W., Oosterloo T. A., 1998, AJ, 115, 162
Majewski S. R., Skrutskie M. F., Weinberg M. D., Ostheimer J. C., 2003, ApJ, 599, 1082
Malhan K., Ibata R. A., Martin N. F., 2018, MNRAS, 481, 3442
Marigo P. et al., 2017, ApJ, 835, 77
Martin N. F., Ibata R. A., Bellazzini M., Irwin M. J., Lewis G. F., Dehnen W., 2004, MNRAS, 348, 12
Martin N. F., Collins M. L. M., Longeard N., Tollerud E., 2018, ApJ, 859, L5
Martinez-Delgado D. et al., 2019, preprint (arXiv:1907.02264)
McClure-Griffiths N. M., Madsen G. J., Gaensler B. M., McConnel D., Schnitzler D. H. F. M., 2010, ApJ, 725, 275
McConnachie A. W., 2012, AJ, 144, 4
McMillan P. J., 2017, MNRAS, 465, 76
Momany Y., Zaggia S., Gilmore G., Piotto G., Carraro G., Bedin L. R., de Angeli F., 2006, A&A, 451, 515
Monaco L., Bellazzini M., Ferraro F. R., Pancino E., 2002, ApJ, 597, L25
Montenegro K., Minniti D., Alonso-García J., Hempel M., Saito R. K., Beers T. C., Brown D., 2019, ApJ, 872, 206
Nidever D. L., Majewski S. R., Butler Burton W., 2008, ApJ, 679, 432
Nidever D. L., Majewski S. R., Butler Burton W., Nigra L., 2010, ApJ, 723, 1618
Price-Whelan A. M., Nidever D. L., Choi Y., Schlafly E. F., Morton S. E., Koposov S. E., Belokurov V., 2019, preprint (arXiv:1811.05991)
Putman M. E. et al., 1998, Nature, 394, 752
Richter P., Fox A. J., Wakker B. P., Howk J. C., Lehner N., Barger K. A., D'Onghia E., Lockman F. J., 2018, ApJ, 865, 145
Robin A. C., Reylè C., Derrière S., Picaud S., 2003, A&A, 409, 523
Russell S. C., Dopita M. A., 1992, ApJ, 384, 508
Sand D. J. et al., 2017, ApJ, 843, 134
Schlafly E. F., Finkbeiner D. P., 2011, ApJ, 737, 103
Schlegel D. J., Finkbeiner D. P., Davis M., 1998, ApJ, 500, 525
Schönrich R., Binney J., Dehnen W., 2010, MNRAS, 403, 1829
Sembach K. R., Howk J. C., Savage B. D., Schull J. M., 2001, AJ, 121, 992
Skowron D. M. et al., 2014, ApJ, 795, 108
Smith G. P., 1963, Bull. Astron. Inst. Neth., 17, 203
Taylor M. B., 2005, in Shopbell P., Britton M., Ebert R., eds, ASP Conf. Ser. Vol. 347, Astronomical Data Analysis Software and Systems XIV. Astron. Soc. Pac., San Francisco, p. 29
Tepper-García T., Bland-Hawthorn J., 2018, MNRAS, 473, 5514
Tepper-García T., Bland-Hawthorn J., Pawlowski M. S., Fritz T. K., 2019, MNRAS, 488, 918
Torrealba G. et al., 2019, MNRAS, 488, 2743
Venzmer M. S., Kerp J., Kalberla P. M. V., 2012, A&A, 547, A12
Wakker B. P., van Woerden H., 1997, ARA&A, 35, 217
Wakker B. P., Oosterloo T. A., Putman M. E., 2002, AJ, 123, 1953
Wang J., Hammer F., Yang Y., Ripepi V., Cioni M.-R. L., Puech M., Flores H., 2019, MNRAS, 486, 5907
Zhang L. et al., 2019, ApJ, 871, 99

This paper has been typeset from a TEX/LATEX file prepared by the author.